Research Article | Vol. 32, No. 7 / 25 Mar 2024 / Optics Express 11673
Optics EXPRESS

Nonlinear asymmetric imaging with AlGaAs metasurface

DAVIDE ROCCO,[1,2,*] ANDREA LOCATELLI,[1,2] LUCA CARLETTI,[1,2] MARIA ANTONIETTA VINCENTI,[1,2] AND COSTANTINO DE ANGELIS[1,2]

[1]Department of Information Engineering, University of Brescia, via Branze 38, 25123 Brescia, Italy
[2]National Institute of Optics-National Research Council (INO-CNR), via Branze 45, 25123 Brescia, Italy
[*]davide.rocco@unibs.it

Abstract: Nowadays, dielectric metasurfaces are a promising platform in many different research fields such as sensing, lasing, all-optical modulation and nonlinear optics. Among all the different kinds of such thin structures, asymmetric geometries are recently attracting increasing interest. In particular, nonlinear light-matter interaction in metasurfaces constitutes a valid approach for achieving miniaturized control over light. Here, we demonstrate nonlinear asymmetric generation of light in a dielectric metasurface via second harmonic generation. By inverting the illumination direction of the pump, the nonlinear emitted power is modulated by more than one order of magnitude. Moreover, we demonstrate how a properly designed metasurface can generate two completely different images at the second harmonic when the direction of illumination is reversed. Our results may pave the way to important opportunities for the realization of compact nanophotonic devices for imaging applications by densely integrating numerous nonlinear resonators.

1. Introduction

Nonlinear metasurfaces are periodic arrangements of meta-atoms which exhibit nonlinear optical responses when exposed to intense light [1,2]. These structures are designed and engineered to manipulate and control light in unconventional ways by taking advantage of nonlinear optical phenomena. Recently, they have been efficiently used in imaging applications, [3–5] meta-lenses [6], infrared up-converters [7,8], wavefront controllers [9] and optical multiplexers [10].

Unlike plasmonic metasurfaces, where the field cannot penetrate inside the meta-atoms, dielectric platforms allow for the enhancement of nonlinear processes by exploiting multipolar Mie resonances in high refractive index materials [11]. Among all the possible semiconductors, aluminum gallium arsenide ($Al_xGa_{1-x}As$) is a quite popular medium for nonlinear optics. Indeed, $Al_xGa_{1-x}As$ possesses a direct gap which increases with the aluminum molar fraction (x) and for x greater than or equal to 0.18 is free from two-photons absorption when operating around the third communication window (i.e. between 1510 nm and 1600 nm). Furthermore, it presents a huge second order nonlinear susceptibility $\chi^{(2)}$ thus making it an ideal candidate for generating second harmonic (SH) light. Indeed, the efficient generation of SH has been demonstrated both numerically and experimentally in AlGaAs metasurfaces [6,12–15]. Due to symmetry considerations, the SH emission from a fully cylindrical AlGaAs resonator is emitted at large angles, which poses a significant limitation for several applications. Conversely, when examining a metasurface composed of the so called 'nano-chairs', the SH light is efficiently radiated in the normal direction due to in-plane symmetry breaking [16,17]. For instance, this concept has been exploited for designing a SH metalens where each nano-chair is associated with a specific SH phase while keeping the transmitted SH amplitude constant [6].

At the same time, dielectric metasurfaces are able to concurrently control both transmitted and reflected nonlinear fields and, therefore, their capability of generating asymmetric nonlinear

#517991 https://doi.org/10.1364/OE.517991
Journal © 2024 Received 8 Jan 2024; revised 14 Feb 2024; accepted 16 Feb 2024; published 14 Mar 2024

Optics EXPRESS

imaging is starting to gain interest [18,19]. In particular, in [18] it has been demonstrated the generation of asymmetric third harmonic from silicon metasurfaces for imaging applications by exploiting nonlinear effects in structures where magneto-electric coupling plays a key role. Nevertheless, since the conversion efficiency decreases with the harmonic order, the generation of second harmonic is expected to be more efficient than the third harmonic.

In this work, we theoretically prove how an AlGaAs platform can generate a strongly asymmetric SH signal as a function of the incident direction, as schematically represented in Fig. 1. In stark contrast with conventional nonlinear devices, here the SH signal is efficiently generated only for one excitation direction and for a specific geometrical parameter set of the metasurface. The asymmetric nature of the SH emission, i.e. the fact that the nonlinear signal can be transmitted or reflected only in one direction, is also referred as nonlinear pseudo-diode [20]. Furthermore, we demonstrate the possibility of realizing a dielectric platform for the creation of complementary images when the pump direction is reversed by properly engineering different metasurface regions in the final device. The proposed design does not require any external control bias and for this reason is directly integrable in several existing optical devices [21]. It is worth noting that, our results can be easily extended to all $\chi^{(2)}$ nonlinear phenomena hence opening new opportunities for the development of compact infrared imaging devices with applications in multi-color imaging systems.

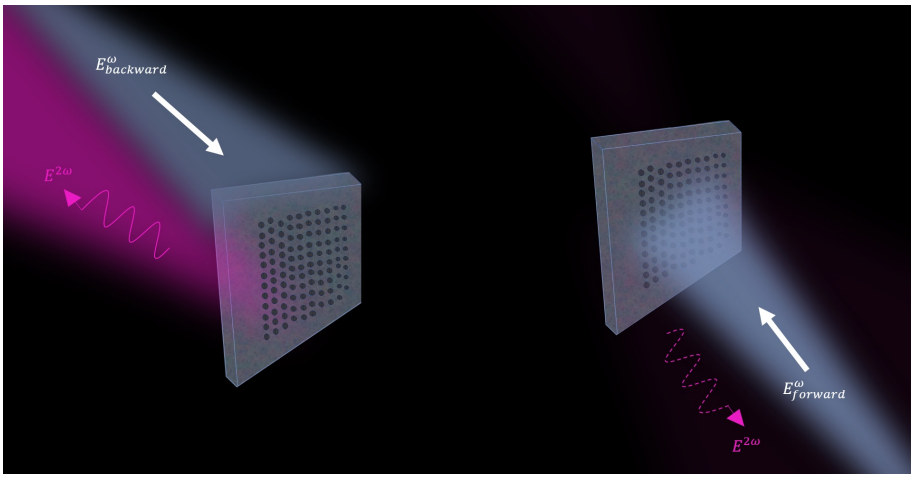

Fig. 1. Concept of nonlinear asymmetric generation in dielectric metasurface. In this sketch, when the incident light is coming from the substrate ($E^{\omega}_{backward}$), the SH signal ($E^{2\omega}$) is strongly emitted in reflection, left panel. When the incident direction is flipped and the source is propagating from the air to the substrate ($E^{\omega}_{forward}$), the emitted SH is negligible, right panel.

2. Results and discussion

Let us consider a metasurface made of AlGaAs nano-chairs placed over a sapphire substrate with a sapphire pedestal in between them as shown in Fig. 2(a). Both the nano-chair and the pedestal are assumed to have an elliptical base with major and minor axes named a and b, respectively. In this work we focus our attention on a metasurface with an elliptical unit cell which allows to exploit more degrees of freedom as compared to the case of a circular one. However, similar results may be obtained for a circular nano-chair by optimizing the other geometrical parameters. The sapphire refractive index is assumed equal to 1.75 whereas for the permittivity dispersion of AlGaAs we apply the analytical model proposed in [22]. Without loss of generality, we fix

Optics EXPRESS

some geometrical parameters by assuming the period P equal to 880 nm (same in both planar directions), the height of the pedestal h_s = 250 nm and the AlGaAs thickness h_c = 400 nm. These initial choices for the geometrical parameters are motivated by the possibility of fabricating the proposed structure in future efforts. The optical performance of the metasurface are evaluated by using finite-element-method simulations in Comsol Multiphysics by simulating the nonlinear radiation coming from our metasurface. The incident light is constituted by a linearly x-polarized plane wave with intensity I_0 = 1 GW/cm^2 and wavelength λ_{inc} = 1.55 μm. Figure 2(b) reports the linear transmittance as a function of the length of the minor axis b when fixing a to 650 nm for the two considered pump direction: forward (when the excitation is coming from the air to the substrate, magenta curve) and backward (light is propagating from the sapphire substrate towards the positive z direction, blue line). As required by reciprocity, the total transmittance remains the same when switching the pump direction. However, the asymmetric nature of the proposed unitary cell leads to different field profile at the pump wavelength inside the nano-chair for the two incident configurations. For instance, when a = 650 nm and b = 700 nm, for forward excitation, the field inside the AlGaAs can be interpreted as a merge between an electric and a magnetic dipolar resonance. Instead, for backward excitation the field resembles an electric dipolar resonance since there is no electric field loop inside the nanoresonator, see the inset of Fig. 2(b). Please note that the different refractive index between AlGaAs ($\approx$ 3.3) and sapphire (1.75) can induce a magneto-electric coupling in the metasurface [23], see the Supplement 1 for more details. Under this condition, it has already been demonstrated that the forward and backward illuminations can lead to enhancement and/or suppression of different multipoles inside the dielectric [18]. To better understand the scattering behaviour of our meta-unit, the optical response is decomposed using a spherical multipole expansion by performing the integration of the induced currents inside the AlGaAs volume [24]. Figure 3(a) displays the obtained dipolar resonances for the two considered pump directions and highlights that the Mie resonances are excited in a different way with forward and backward excitation, which we mainly ascribe with their magneto-electric coupling [25,26]. Around b = 700 nm, for backward excitation an electric dipole contribution is predominantly excited inside the nano-chair whereas a sizable magnetic dipole is clearly observed for forward incidence.

The observed changes in the multipolar contributions inside the nano-chair lead to different SH for the two pump directions. This concept is the fundamental principle of nonlinear optical isolators [27–32]. Indeed, our device is reciprocal when the nonlinearities are not considered. However, since the geometry and the permittivity are spatially asymmetric, the electromagnetic field concentrates at different positions for forward or backward incidence. Therefore, when the nonlinearity are considered, the forward and backward pumps induce different distributions of nonlinear currents that have a different coupling with the metasurface modes at the SH. As a consequence, it is possible to design a metasurface that exhibits high SH for an input backward signal, while keeping low the nonlinear emission for forward pumps or viceversa. For each unit-cell geometry, BFPR is defined as the ratio between the SH power emitted in reflection when the metasurface is excited with backward incidence with respect to the SH radiated for forward input light. Interestingly, when b = 700 nm, the SH backward-to-forward power ratio (BFPR) reaches its maximum equal to 25. The nonlinear simulations are also performed in Comsol Multiphysics following the same approach reported in [15]. In details, we first compute the fields at the fundamental frequency to describe the SH sources in terms of current densities, J_i. Since AlGaAs is a zincblende crystal, the i-th component of the external current density is computed as: $J_i = j\omega_{SH}\epsilon_0\chi^{(2)}E_{FF,j}E_{FF,k}$ with $i \neq j \neq k$, where ϵ_0 is the vacuum permittivity, $E_{FF,i}$ is the i-th component of the electric field at the fundamental frequency and $\chi^{(2)}$ is the nonlinear second-order susceptibility, which we assume to be equal to 100 pm/V [15]. A description of the simulation methodology can be found in the Supplement 1. The SH efficiency, η, is defined as

Optics EXPRESS

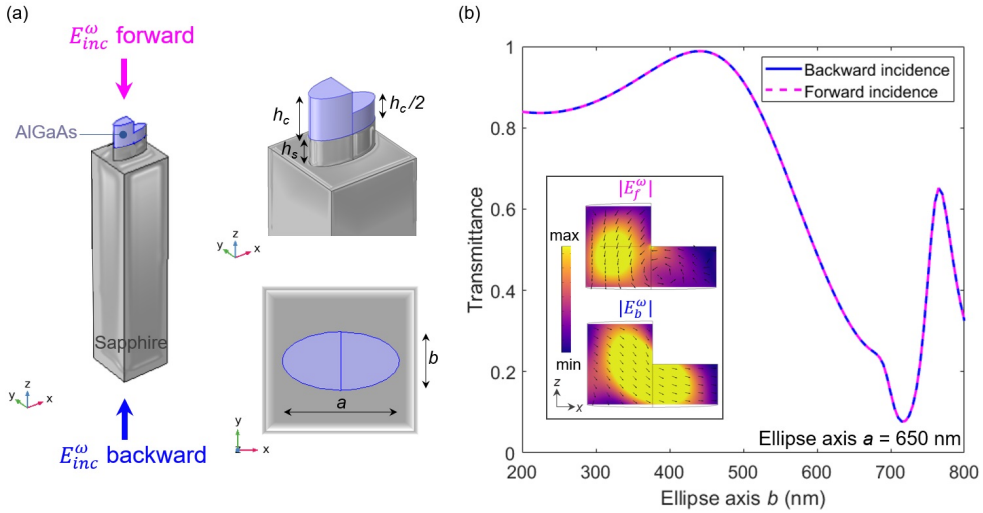

Fig. 2. (a) The unit cell of the AlGaAs metasurface. (b) Transmittance as a function of the ellipse axis b at a wavelength of 1.55 μm computed in the case of a pump with backward (blue curve) or forward (magenta) incidence for a metasurface with period of 880 nm, a = 650 nm, h_c = 400 nm, h_s = 250 nm. The inset color-maps display the electric field magnitude inside the same nano-chair (a = 650 nm, b = 700 nm) when switching the pump direction. The black arrows represent the electric field components.

$P^{2\omega}/P^{\omega}$, being $P^{2\omega}$ the scattered SH in reflection considering all the diffraction orders and P^{ω} the incident power at the fundamental wavelength.

We study the emitted SH efficiency as a function of the nano-chair ellipticity for the two considered pump directions. The maps reported in Fig. 4 are obtained by keeping fixed the pump wavelength at 1.55 μm and the period at 880 nm. For completeness, in the Supplement 1 we also report the scattered SH in transmission. For the above considerations, the SH power changes for different incident direction. Interestingly, we can identify three different zones named A, B and C, see Fig. 4. Point A, which corresponds to a metasurface with a = 650 nm and b = 700 nm, is associated with a strongly emitted SH solely for the case of backward incidence (BRPR = 25). For this pump excitation, the SH reaches its maximum efficiency equal to $2.2\text{x}10^{-4}$ while it only reaches $8.78\text{x}10^{-6}$ for the forward incidence. Contrarily, point B (a = 750 nm, b = 720 nm), is associated with a metasurface generating the SH signal mainly when the incident light is propagating from the air region to the substrate (i.e. forward incidence) reaching the maximum SH efficiency of $4.4\text{x}10^{-4}$. For point B, η is equal to $2.17\text{x}10^{-5}$ for the backward incidence with a SH BFPR equal to 0.0493. Point C instead identifies a metasurface where the SH emission is negligible for both excitation directions (i.e. $\eta<10^{-6}$, SH BFPR $\approx$ 1.98). Therefore, it is possible to identify three metasurfaces with different nonlinear signal emission behaviors which can act as building blocks for the generation of asymmetric images at the SH wavelength when combined for the creation of the final device. Figure 4(c) summarizes the computed emitted SH efficiency as a function of the pump direction for the three considered cases. Please note that the pedestal height is selected to guarantee good regions identification in terms of asymmetric SH scattered power when reversing the incident pump direction. We numerically verified that a pedestal of 250 nm is the minimum value to obtain such behaviour, see Supplement 1. However, a complete study of all the geometrical space is outside the main purpose of this manuscript. Let us underline that asymmetric SH emission due to the magneto-electric coupling from the difference in the refractive indices between AlGaAs and sapphire is also achievable in metasurfaces with a fully

Optics EXPRESS

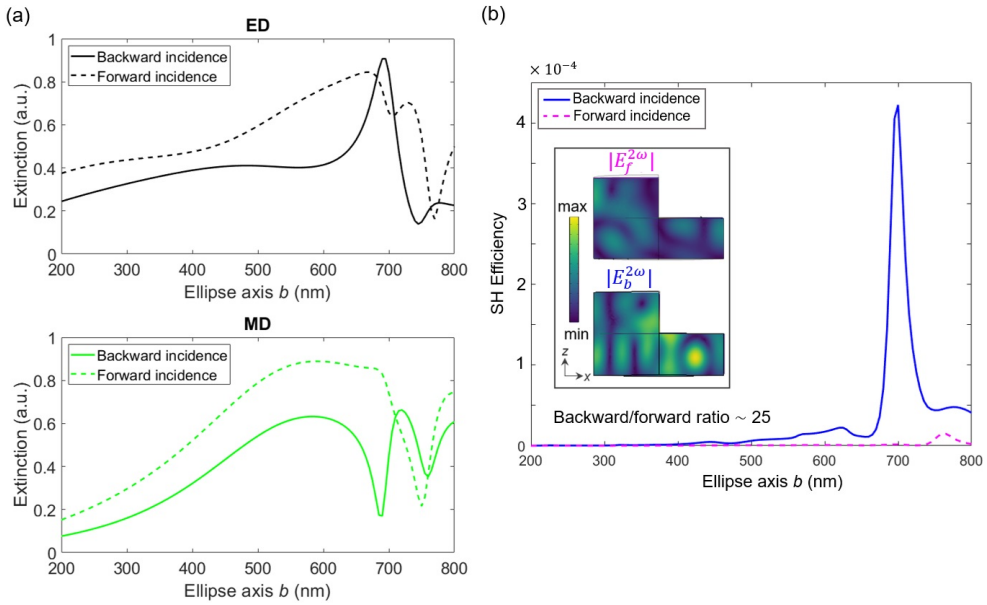

Fig. 3. (a) Multipolar scattering decomposition of the electromagnetic field inside the AlGaAs nano-chair at a wavelength of 1.55 μm as a function of the ellipse axis b for the two considered pump directions. The top panel displays the electric dipolar (ED) contribution while the bottom panel reports the magnetic dipolar (MD) one. The incident light is a plane wave linearly polarized along the x-axis. (b) The emitted SH efficiency when the pump direction is switched from backward (blue line) to forward incidence (magenta line) as a function of the ellipse axis b. The backward-to-forward SH power ratio reaches the maximum value of 25 when b = 700 nm. The insets display the SH field magnitude inside the nano-chair with a = 650 and b = 700 nm for the two pump directions.

cylindrical meta-unit. The reported use of the nano-chairs is instead necessary for achieving a predominant SH emission in the zero diffraction order. A complete analysis of the SH radiation pattern from such structures in comparison with the fully cylindrical ones is reported in [6,16].

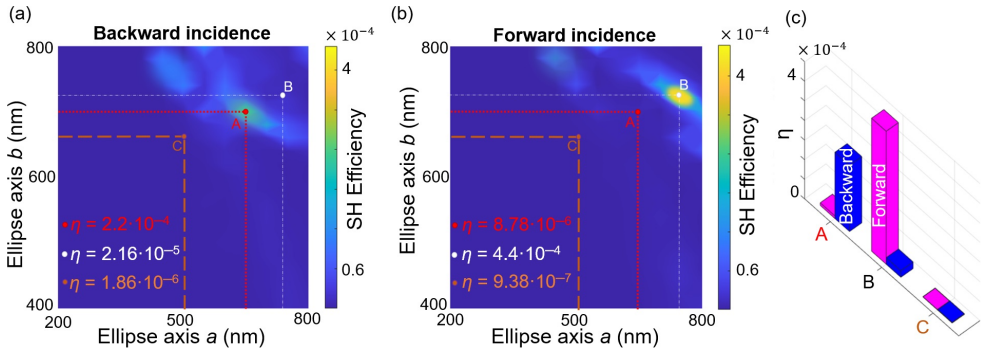

Fig. 4. The emitted SH efficiency as a function of the ellipse axes a and b for pump with (a) backward or (b) forward incidence, respectively. (c) The SH efficiency for the metasurfaces A, B and C for the backward (blue) or forward (magenta cuboids) incident pump direction.

We provide a potential application of the designed metasurface for asymmetric image generation. The target images are reported in Fig. 5. In details, Fig. 5(a) displays the generation of an image

Optics EXPRESS

for backward incidence and its complementary one when reversing the pump direction. Both images are assumed to be detected in reflection. The two images of Fig. 5(a) are obtained by solely using regions α and β which correspond to finite areas with unit-cell geometry as A and B, respectively. Region β is assumed to have a total dimension of 15x15 μm^2 and it is surrounded by region α up to the maximum dimension of the total structure which is assumed to be 30x30 μm^2. Instead, Fig. 5(b) shows the possibility of creating more sophisticated asymmetric SH images when considering also region γ with unit-cell geometry as C. In this case, the symbol '+' appears for backward incidence whereas the sign '−' is formed for the other pump direction. Here, the building blocks are equally considered with a size of 15x15 μm^2 leading to a final platform with total dimensions of 60x45 μm^2. The block must be sufficiently large for the second harmonic signal to perceive it as infinite, mimicking the assumption made in the simulation where the metasurface is considered infinitely extended. As reported in [18] a dimension of the order of few tens μm^2 is reasonable. The images are computed by considering the SH field emission coming from the associated block with peak intensity as computed in Fig. 4, neglecting any coupling effects. Although very schematic, the results show the potential of the proposed structure for the generation of nonlinear images. Furthermore, in [6,33] we have already demonstrated the good accordance between simulations and experiments in terms of SH emission pattern in similar structures. Thus, we hold strong confidence that the theoretical findings presented in this research could be effectively validated through experimental testing in a future effort.

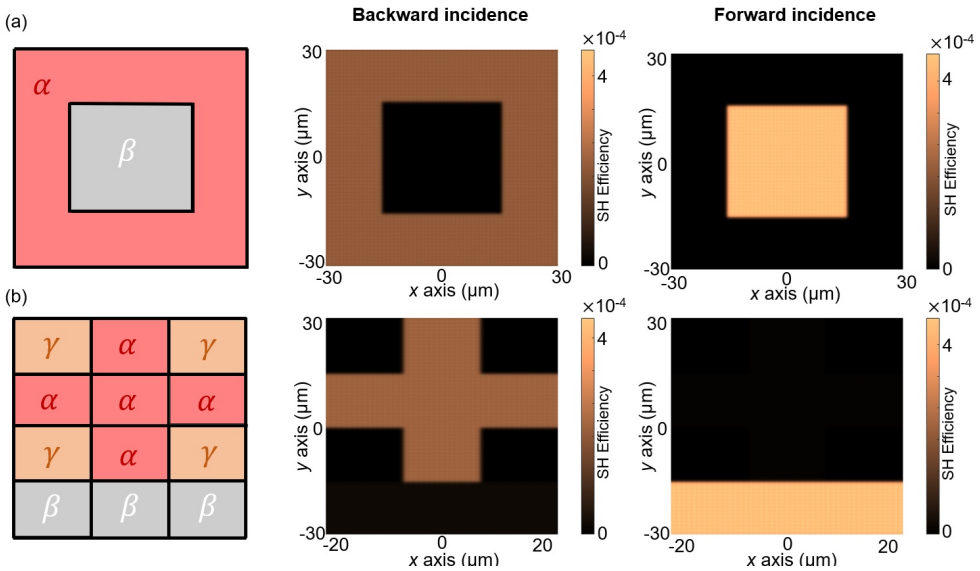

Fig. 5. (a) An example of generation of complementary SH images as a function of the pump direction when using regions α and β. (b) Example of three-level images obtained when considering also region γ in the realization of the final platform.

To conclude, in this work, we prove thin dielectric metasurfaces with large asymmetric response for free-space radiation based on nonlinear process. Differently from Kerr-like mechanism where the dynamics of the nonlinear generated signal is at least of the order of hundreds of nanoseconds [32], our approach based on $\chi^{(2)}$ harmonic generation can be considered instantaneous thus allowing ultra-fast nonlinear imaging generation.

Optics EXPRESS

3. Conclusion

In this work, we have shown the possibility of creating nonlinear asymmetric patterns with AlGaAs metasurfaces when switching the pump direction. We focus on $\chi^{(2)}$ nonlinear phenomena such as second harmonic generation. Specifically, the proposed structure is able to profitably generate asymmetric images with a nonlinear efficiency up to $4.4\text{x}10^{-4}$ for a pump intensity of 1 GW/cm^2. Our findings, which can find applications in different fields such as optical encryption, nonlinear QR codes and imaging systems, pave the way for the development of metasurfaces governed by the interplay between asymmetric meta-atoms, magneto-electric coupling and nonlinear light-matter interactions. This will lead to the asymmetric and independent control of different electromagnetic parameters such as the amplitude, the phase, and the polarization of the emitted nonlinear signals.

Funding. Ministero dell'Università e della Ricerca (PRIN 2020, PRIN 2022, PRIN 2022, PRIN 2022, PRIN 2022, PRIN PNRR 2022, project DOSE (2022MANFK5), project FLAIRS (P2022RFF9K), project FLAIRS (P2022RFF9K) Next generation EU, project GRACE6G (2022H7RR4F), project METEOR (2020EY2LJT), project NO LIMITHz (2022BC5BW5), project PILLARS (2022YJ5AZH)).

Acknowledgments. The authors thank NATO SPS Grant no. G5984 - RESPONDER for financial support. The authors also acknowledge financial support by the European Union – Next Generation EU - PRIN PNRR 2022 project FLAIRS (P2022RFF9K), PRIN 2022 project DOSE (2022MANFK5), PRIN 2022 project GRACE6G (2022H7RR4F), PRIN 2022 project NO LIMITHz (2022BC5BW5), PRIN 2022 project PILLARS (2022YJ5AZH), PRIN 2020 project METEOR (2020EY2LJT).

Disclosures. The authors declare no conflicts of interest.

Data availability. Data underlying the results presented in this paper are not publicly available at this time but may be obtained from the authors upon reasonable request.

Supplemental document. See Supplement 1 for supporting content.

References

1. A. Krasnok, M. Tymchenko, and A. Alù, "Nonlinear metasurfaces: a paradigm shift in nonlinear optics," Mater. Today **21**(1), 8–21 (2018).
2. G. Li, S. Zhang, and T. Zentgraf, "Nonlinear photonic metasurfaces," Nat. Rev. Mater. **2**(5), 17010 (2017).
3. S. Keren-Zur, L. Michaeli, H. Suchowski, *et al.*, "Shaping light with nonlinear metasurfaces," Adv. Opt. Photonics **10**(1), 309–353 (2018).
4. C. Schlickriede, S. S. Kruk, and L. Wang, "Nonlinear imaging with all-dielectric metasurfaces," Nano Lett. **20**(6), 4370–4376 (2020).
5. Y. Gao, Y. Fan, and Y. Wang, "Nonlinear holographic all-dielectric metasurfaces," Nano Lett. **18**(12), 8054–8061 (2018).
6. C. Gigli, G. Marino, and A. Artioli, "Tensorial phase control in nonlinear meta-optics," Optica **8**(2), 269–276 (2021).
7. R. Camacho-Morales, D. Rocco, and L. Xu, "Infrared upconversion imaging in nonlinear metasurfaces," Adv. Photonics **3**(03), 036002 (2021).
8. G. Grinblat, "Nonlinear dielectric nanoantennas and metasurfaces: frequency conversion and wavefront control," ACS Photonics **8**(12), 3406–3432 (2021).
9. B. Liu, B. Sain, and B. Reineke, "Nonlinear wavefront control by geometric-phase dielectric metasurfaces: influence of mode field and rotational symmetry," Adv. Opt. Mater. **8**(9), 1902050 (2020).
10. M. Ma, Z. Li, and W. Liu, "Optical information multiplexing with nonlinear coding metasurfaces," Laser Photonics Rev. **13**(7), 1900045 (2019).
11. V. Zubyuk, L. Carletti, M. Shcherbakov, *et al.*, "Resonant dielectric metasurfaces in strong optical fields," APL Mater. **9**(6), 060701 (2021).
12. D. Rocco, L. Carletti, and R. Caputo, "Switching the second harmonic generation by a dielectric metasurface via tunable liquid crystal," Opt. Express **28**(8), 12037–12046 (2020).
13. D. Rocco, A. Zilli, and A. Ferraro, "Tunable second harmonic generation by an all-dielectric diffractive metasurface embedded in liquid crystals," New J. Phys. **24**(4), 045002 (2022).
14. S. Liu, M. B. Sinclair, and S. Saravi, "Resonantly enhanced second-harmonic generation using iii–v semiconductor all-dielectric metasurfaces," Nano Lett. **16**(9), 5426–5432 (2016).
15. V. F. Gili, L. Carletti, and A. Locatelli, "Monolithic algaas second-harmonic nanoantennas," Opt. Express **24**(14), 15965–15971 (2016).
16. D. Rocco, C. Gigli, L. Carletti, *et al.*, "Vertical second harmonic generation in asymmetric dielectric nanoantennas," IEEE Photonics J. **12**(3), 1–7 (2020).

Optics EXPRESS

17. D. Rocco, M. Gandolfi, and A. Tognazzi, "Opto-thermally controlled beam steering in nonlinear all-dielectric metastructures," Opt. Express **29**(23), 37128–37139 (2021).
18. S. S. Kruk, L. Wang, and B. Sain, "Asymmetric parametric generation of images with nonlinear dielectric metasurfaces," Nat. Photonics **16**(8), 561–565 (2022).
19. E. Mobini, R. Alaee, R. W. Boyd, *et al.*, "Giant asymmetric second-harmonic generation in bianisotropic metasurfaces based on bound states in the continuum," ACS Photonics **8**(11), 3234–3240 (2021).
20. S. Boroviks, A. Kiselev, K. Achouri, *et al.*, "Demonstration of a plasmonic nonlinear pseudodiode," Nano Lett. **23**(8), 3362–3368 (2023).
21. M. Cotrufo, S. A. Mann, H. Moussa, *et al.*, "Nonlinearity-induced nonreciprocity—part i," IEEE Trans. Microwave Theory Tech. **69**(8), 3569–3583 (2021).
22. S. Gehrsitz, F. Reinhart, and C. Gourgon, "The refractive index of al_x ga_{1-x} as below the band gap: accurate determination and empirical modeling," J. Appl. Phys. **87**(11), 7825–7837 (2000).
23. A. E. Miroshnichenko, A. B. Evlyukhin, Y. S. Kivshar, *et al.*, "Substrate-induced resonant magnetoelectric effects for dielectric nanoparticles," ACS Photonics **2**(10), 1423–1428 (2015).
24. P. Grahn, A. Shevchenko, and M. Kaivola, "Electromagnetic multipole theory for optical nanomaterials," New J. Phys. **14**(9), 093033 (2012).
25. M. Albooyeh, V. Asadchy, and R. Alaee, "Purely bianisotropic scatterers," Phys. Rev. B **94**(24), 245428 (2016).
26. Y. Ra'di and S. A. Tretyakov, "Balanced and optimal bianisotropic particles: maximizing power extracted from electromagnetic fields," New J. Phys. **15**(5), 053008 (2013).
27. Y. Shi, Z. Yu, and S. Fan, "Limitations of nonlinear optical isolators due to dynamic reciprocity," Nat. Photonics **9**(6), 388–392 (2015).
28. L. Fan, J. Wang, and L. T. Varghese, "An all-silicon passive optical diode," Science **335**(6067), 447–450 (2012).
29. J. Wang, L. Fan, and L. T. Varghese, "A theoretical model for an optical diode built with nonlinear silicon microrings," J. Lightwave Technol. **31**(2), 313–321 (2013).
30. C. Caloz, A. Alu, and S. Tretyakov, "Electromagnetic nonreciprocity," Phys. Rev. Appl. **10**(4), 047001 (2018).
31. D. L. Sounas and A. Alu, "Nonreciprocity based on nonlinear resonances," Antennas Wirel. Propag. Lett. **17**(11), 1958–1962 (2018).
32. M. Cotrufo, A. Cordaro, D. L. Sounas, *et al.*, "Passive bias-free non-reciprocal metasurfaces based on thermally nonlinear quasi-bound states in the continuum," Nat. Photonics **18**(1), 81–90 (2024).
33. G. Marino, D. Rocco, and C. Gigli, "Harmonic generation with multi-layer dielectric metasurfaces," Nanophotonics **10**(7), 1837–1843 (2021).